Nuclear Engineering and Design 429 (2024) 113656

Contents lists available at ScienceDirect

Nuclear Engineering and Design

journal homepage: www.elsevier.com/locate/nucengdes

Development of the ENIGMA fuel performance code for LWR applications with chromium-coated cladding

Glyn Rossiter [a,1], Kerr Fitzgerald [b], Aiden Peakman [a,c,d,*]

[a] National Nuclear Laboratory, Warrington WA3 6AE, UK
[b] University of Central Lancashire, Fylde Rd, Preston PR1 2HE, UK
[c] University of Manchester, Manchester M13 9PL, UK
[d] University of Liverpool, Liverpool, Merseyside L69 3GH, UK

ARTICLE INFO

Keywords:
Fuel performance
ATF
ENIGMA
LOCA
Chromium-coated
Accident Tolerant Fuel

ABSTRACT

Zirconium-alloy cladding with a chromium coating is the most advanced of the near-term concepts amongst Accident Tolerant Fuel (ATF) materials for Light Water Reactor (LWR) applications. The ENIGMA fuel performance code has been updated to model the thermo-mechanical behaviour of such cladding in both normal and off-normal operating conditions. The focus was on accurately simulating the behaviour in Loss Of Coolant Accident (LOCA) conditions to evaluate the increase in coping time during design-basis accidents. New low-temperature and high-temperature models were incorporated for cladding oxidation and hydriding and cladding creep which take into account the impact of the chromium coating on the overall cladding behaviour. Furthermore, the consumption of the chromium coating due to high-temperature diffusion of chromium into the cladding base alloy's β-Zr phase is simulated. The new models have been validated using measurements on chromium-coated cladding from irradiated rods, high-temperature annealing experiments and semi-integral LOCA tests. The validation showed good agreement between ENIGMA's predictions and the experimental data; thereby demonstrating the applicability of the new models for simulating the performance of LWR fuel rods with chromium-coated cladding in both normal operation and accident conditions.

1. Introduction

Light Water Reactors (LWRs) play a vital role in the global nuclear fleet, accounting for over 80 % of currently operating nuclear reactors (WNA, 2024a). They will continue to be the predominant reactor technology for several decades, thanks to their proven track record, regulatory familiarity and flexible operation characteristics that support decarbonisation efforts and renewable grid integration (WNA, 2024b; NEA, 2021; Hadri et al., 2021). Hence, the development of technologies that underpin the safety and performance of LWRs (particularly fuel forms) is critical for the future low-carbon energy system.

Zirconium alloys have been extensively used as cladding materials for LWR nuclear fuel rods due to their favourable mechanical properties and low neutron absorption cross-section. However, during Loss-Of-Coolant Accidents (LOCAs), zirconium alloy cladding undergoes significant high-temperature oxidation, leading to substantial hydrogen gas generation. This can degrade safety performance characteristics, as evidenced by the Fukushima Daiichi accident. To mitigate such risks, several Accident Tolerant Fuel or Advanced Technology Fuel (ATF) cladding materials have been proposed. These new material concepts, such as chromium-coated zirconium alloys, can increase the 'coping time' in accident scenarios by enhancing high-temperature oxidation resistance and reducing hydrogen generation and embrittlement, thereby maintaining structural integrity longer during accident conditions.

ATF cladding materials can be broadly categorised into long-term concepts, which involve replacing zirconium alloys with new materials, and near-term concepts, which focus on applying coatings to the surface of zirconium alloys. Among the near-term ATF cladding concepts, chromium-coated zirconium alloys are the most advanced (Yang et al., 2022). Chromium coatings exhibit excellent chemical stability and form a protective Cr_2O_3 layer during high-temperature oxidation under LOCA conditions. This Cr_2O_3 layer significantly slows oxidation and reduces hydrogen gas generation (Brachet et al., 2019; Steinbrück et al.,

* Corresponding author at: University of Manchester, Manchester, M13 9PL, UK.
E-mail address: aiden.peakman@manchester.ac.uk (A. Peakman).
[1] Current address: Westinghouse Electric UK, Springfields, Salwick, Preston PR4 0XJ, UK.

https://doi.org/10.1016/j.nucengdes.2024.113656
Received 4 August 2024; Received in revised form 11 October 2024; Accepted 17 October 2024
Available online 22 October 2024

2011). Chromium coatings also decrease hydrogen absorption within the underlying zirconium alloy, reducing hydrogen-induced clad embrittlement, both under low-temperature normal operation conditions and high-temperature fault conditions. Moreover, the higher intrinsic creep resistance of chromium compared to zirconium (Hazan et al., 2021), combined with the increased oxidation resistance and reduced embrittlement, is expected to result in chromium-coated zirconium alloy cladding having high residual strength and ductility in LOCA conditions (Yook et al., 2022).

For any new fuel form, it is crucial to predict its thermo-mechanical behaviour in order to assess its performance against various safety limits. In the UK, the primary computer code for predicting fuel thermo-mechanical behaviour is ENIGMA. This code models the evolution of the thermal and mechanical state of a fuel rod, in part via simulation of the underlying fuel microstructure (including the generation and redistribution of fission gas) and its evolution (Rossiter, 2011). The main purpose of ENIGMA is to determine various output parameters, including stresses, temperatures, strains and corrosion layer thicknesses, which are then compared with the aforementioned safety limits. Versions of the ENIGMA code in the UK are maintained and developed by EDF Energy and the National Nuclear Laboratory (NNL). For this study, the NNL version, specifically ENIGMA 7.8P6, has been used.

Given the importance of chromium-coated fuel as an ATF concept, a number of fuel performance codes, such as BISON and TRANSURANUS, have added capabilities to model these fuel forms (Wagih et al., 2018; Sweet et al., 2022; Aragon et al., 2025). BISON has demonstrated the benefits of chromium coatings in improving oxidation resistance and structural integrity during both steady-state and transient conditions (Wagih et al., 2018). Similarly, TRANSURANUS has been extended to simulate the behaviour of chromium-coated cladding, showing enhanced performance under accident scenarios (Aragon et al., 2025).

Having multiple codes with similar capabilities, such as ENIGMA, is essential for independent verification and cross-validation of results, as different codes are often based on distinct physical models and numerical methods. Adding new ATF capabilities to ENIGMA not only ensures alignment with other state-of-the-art fuel performance codes but also provides a more robust and diverse toolset for evaluating the performance of advanced cladding materials like chromium-coated fuel.

The ENIGMA fuel performance code already simulates a range of fuel forms relevant to light water reactors, including UO_2, (U,Pu)O_2, (U,Th)O_2, U_3Si_2 and inert matrix fuel (Peakman et al., 2022; Rossiter, 2011). It is also capable of simulating various cladding materials, including Zircaloy-2, Zircaloy-4, ZIRLO®, Optimized ZIRLO™ and M5® (Rossiter and Peakman, 2024). This fuel and cladding simulation capability has been supplemented by recent enhancements to model UO_2-Mo fuel and chromium-coated cladding. The former is described by Peakman and Rossiter (2024), while the latter is detailed in this paper.

The new models for chromium-coated cladding include models for low-temperature and high-temperature cladding oxidation and hydriding (as described in Section 2.1), coating consumption due to chromium diffusion into the cladding base alloy's β-Zr phase at high temperatures (see Section 2.2), and low-temperature and high-temperature cladding creep (discussed in Section 2.3). The new models have been validated using measurements on chromium-coated cladding from irradiated rods, high-temperature annealing experiments and semi-integral LOCA tests (as explained in Section 3).

2. Model development

2.1. Model for cladding oxidation and hydriding

There is a significant amount of measured data on the oxidation of Cr-coated cladding in water or steam in the open literature. However, the majority of this is for normal operation cladding temperatures (~300 °C) when oxidation is universally found to be minimal (Bischoff et al., 2018) (Krejčí et al., 2020; Bischoff et al., 2016). Thus, such data cannot be used to develop an oxidation model for Cr-coated cladding. The remaining data are for cladding temperatures in the range of peak values experienced during LOCAs (~800 to 1200 °C). However, most of these remaining data are for two-sided oxidation, where the low oxidation of Cr at the outer (coated) surface is dominated by the high oxidation of Zr at the inner (uncoated) surface, and/or for a single temperature. So, again, these data cannot be used to develop an oxidation model for Cr-coated cladding. Hence, the single-sided (sealed tubes) oxidation data for Framatome's Cr-coated M5® cladding tested at 800, 1000 and 1100 °C, as published in their EATF Phase 2 programme final report (Cross, 2018), represent a potentially unique resource (at the current time) for oxidation model development. These data – as reproduced in Fig. 1 – have therefore been used here to develop a basic oxidation model. Given the oxidation data used in the model development, the model is nominally specific to the Cr coating technique used by Framatome and applicable only for high-temperature oxidation in steam. However, it is used here as a general Cr-coated cladding oxidation model which can also be applied for low-temperature oxidation in water (normal operation conditions). The model reproduces the observed behaviour at low temperatures, i.e. minimal (less than one micron oxide thickness) oxidation for typical irradiation times of several years.

The Framatome data are consistent with oxidation of the Cr coating (to form Cr_2O_3) following a parabolic rate law (which in turn is consistent with oxidation being limited by the rate of diffusion of oxygen through the oxide layer). Using the parabolic rate law from Ref. (Rossiter and Peakman, 2024) we have:

$$\frac{dw}{dt} = \frac{K_p}{2w}, K_p = C_p exp\left(-\frac{Q}{RT}\right) \quad (1)$$

where w is the weight gain per unit surface area, K_p is the so-called parabolic rate constant (which is actually temperature dependent), t is time, C_p is a constant, Q is the activation energy for oxidation, R is the molar gas constant, T is the absolute temperature at the clad metal-oxide interface, and dw/dt is the rate of weight gain per unit surface area.

Values for K_p at 800, 1000 and 1100 °C were obtained by performing linear regression fits of the corresponding w^2 versus t data: the results were 2.2401×10^{-6}, 6.9789×10^{-5} and 6.0973×10^{-4} $mg^2\ cm^{-4}\ s^{-1}$, respectively. The ln K_p values were then plotted against inverse temperature, and a linear regression fit to the three datapoints gave an intercept of 11.804484 $mg^2\ cm^{-4}\ s^{-1}$ and a gradient of −26740 K. It follows that $C_p = exp(11.804484) = 133851\ mg^2\ cm^{-4}\ s^{-1}$, or 0.133851 $g^2\ cm^{-4}\ s^{-1}$, and Q/R = 26740 K.

The new ENIGMA oxidation model for Cr-coated cladding

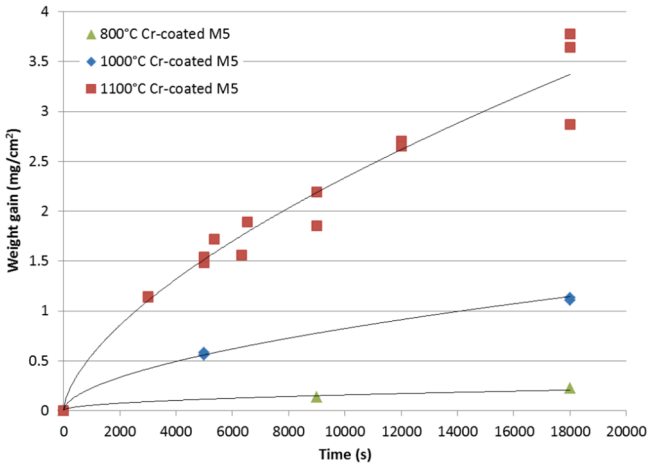

Fig. 1. Single-sided oxidation (weight gain per unit surface area) measurements for Framatome Cr-coated cladding at 800, 1000 and 1100 °C (Cross, 2018).

implements Equation (1) with the C_p and Q/R values just defined for outer surface oxidation (but not inner surface oxidation) of all clad base alloys while the Cr has not been fully consumed. Once fully consumed, outer surface oxidation is computed via the existing (low- and high-temperature) models for the relevant clad base alloy.[2] The Cr is taken to be fully consumed when the outer surface oxide thickness is greater than or equal to the initial coating thickness multiplied by the Pilling-Bedworth ratio for the oxidation of Cr to Cr_2O_3 minus the beginning-of-life oxide thickness.[3] Based on Cr and Cr_2O_3 densities of 7140 kg m^{-3} (National Institutes of Health (2021a)) and 5220 kg m^{-3} (National Institutes of Health (2021a)), the Pilling-Bedworth ratio is set to 2.00 (compare with 1.56 for the oxidation of Zr to ZrO_2).

For consistency with the uncoated cladding oxidation models: (a) weight gain rates per unit surface area are evaluated in mg dm^{-2} d^{-1} (milligrams per decimetre squared per day); (b) weight gains per unit surface area are not used directly; instead, they are indirectly calculated from the start-of-substep oxide thickness in metres using a conversion factor of $16.5x10^6$ mg dm^{-2} m^{-1} (milligrams per decimetre squared per metre); and (c) oxide growth rates in m s^{-1} (metres per second) are calculated from the computed weight gain rates per unit surface area in mg dm^{-2} d^{-1} by dividing by the same conversion factor and by 86400 s d^{-1} (seconds per day). Note that the conversion factor under (b) is different to that for oxidation of Zr used in the other cladding oxidation models.

Any Cr_2O_3 produced is treated as high-temperature oxide irrespective of whether it was generated at low or high temperatures. Thus, the modelling of outer surface oxidation of Zr once the Cr is fully consumed treats the Cr_2O_3 as existing high-temperature oxide in the application of the weight gain differential equation. This implicitly assumes that the Cr_2O_3 formed has the same oxygen transport properties as ZrO_2 and is opaque to steam.

Clad hydriding of uncoated cladding is not modelled explicitly in ENIGMA: instead, hydrogen pickup is calculated, and the hydrogen content averaged over the wall thickness is computed. In the case of Cr-coated cladding, this same approach is taken, but hydrogen is only assumed to be picked up when Zr (not Cr) is oxidising, and the hydrogen content is averaged over the thickness of the cladding base alloy, not the combined wall thickness of the base alloy and coating.[4] The hydrogen pickup of the base alloy is modelled as per uncoated cladding.

Introduction of the new Cr-coated cladding oxidation and hydriding model into ENIGMA required some enabling functionality to be added for modelling Cr-coated cladding, in particular:

- the existing low-temperature (normal operation) clad outer surface oxidation model for base alloys in PWR conditions was modified such that: (a) the transition from a parabolic/cubic to linear rate law only occurs when the ZrO_2 thickness exceeds the existing transition value; and (b) the oxidation rate enhancement due to lithium precipitation in the oxide only occurs when the ZrO_2 thickness exceeds the existing threshold value
- the calculation of oxygen weight fraction in the cladding in the clad burst stress model was modified such that only oxygen in ZrO_2 (not oxygen in Cr_2O_3) is taken into account
- the calculation of equivalent cladding reacted (ECR) was modified such that only consumption of the base alloy metal (not consumption of the coating) is taken into account, and such that the relevant reference wall thickness is the effective wall thickness of the base alloy after

2.2. Model for coating thinning due to chromium diffusion

The new model for coating thinning due to diffusion simulates diffusion of chromium from the coating into the β-Zr layer of the base alloy at high temperature (for example, during a LOCA). This phenomenon has been shown to be as important as clad oxidation for coating thinning during high-temperature transients: at 1200 °C the rate of coating thinning due to chromium diffusion is almost identical to the rate of coating thinning due to oxidation (Brachet et al., 2019). Thus, to accurately determine the 'coping time' benefit of ATF with Cr-coated cladding during high-temperature accidents requires both coating oxidation and chromium diffusion to be modelled.

The modelling assumes diffusion of chromium from the coating to the base alloy. In reality, a $ZrCr_2$ intermetallic layer forms between the coating and the base alloy at the high Cr weight percentages immediately adjacent to the base alloy-coating interface (Yang et al., 2021). Thus, the diffusion process as a whole involves diffusion of chromium from the coating into the $ZrCr_2$ layer (which grows as chromium diffuses into it),[5] diffusion of Cr through the $ZrCr_2$ layer, and diffusion of Cr through the base alloy from the $ZrCr_2$ layer. The Cr coating can also reform once it has been consumed via reduction of the coating oxide (Cr_2O_3) layer (Yang et al., 2022), and the cladding thermochemistry is complicated by formation of a Zr-Cr eutectic above ~1300 °C (Brachet et al., 2020a). However, (a) the $ZrCr_2$ layer is relatively thin, and its presence does not affect the Cr weight percentages in the base alloy; (b) the decrease in oxidation rate due to the increasing thickness of the reformed Cr coating is offset to some extent by the increase in oxidation rate due to the decreasing thickness of the Cr_2O_3 layer, and ignoring the reformation is conservative from the perspective of demonstrating clad integrity; and (c) the eutectic formation is effectively a failure mechanism to be avoided in design-basis accidents[6] rather than to be modelled (like clad melting). With respect to (a), the modelling approach taken effectively models the Cr and $ZrCr_2$ layers as a combined Cr layer. This implicitly assumes that the $ZrCr_2$ layer has thermo-mechanical properties and oxidation behaviour comparable to that of the Cr coating, which is reasonable given its thinness and intermetallic nature.

Given the large radius to thickness ratio of the base alloy, the chromium diffusion in an isothermal anneal for time t at absolute temperature T can be accurately predicted by an analytical solution of the 1-D time-dependent diffusion equation in Cartesian coordinates subject to the appropriate boundary conditions (Brachet, et al., 2019). That is,

$$\frac{\partial C}{\partial t} = D\frac{\partial^2 C}{\partial x^2} \tag{2}$$

can be solved, assuming a semi-infinite medium, subject to boundary conditions $C(x > 0,0) = C_{init}$ and $C(0,t) = C_s$, where $C = C(x,t)$ is the chromium concentration (atoms per unit volume) at time t at a distance x from the coating-base alloy interface, $D = D(T)$ is the diffusion

[2] Both the pre- and post-consumption oxidation behaviour modelled are simplified given the parabolic growth data used to develop the model. The complexities of behaviour observed by Brachet et al (2020) due to the effects of formation of a $ZrCr_2$ layer and subsequent transformation into Cr and ZrO_2 are not simulated.

[3] The beginning-of-life (i.e. beginning of irradiation) oxide thickness is subtracted because it is assumed that the initial coating thickness (input parameter) is the as-manufactured value after any (very rapid, but limited) out-of-reactor oxidation (which occurs during the manufacturing process itself).

[4] In BWR conditions, the clad hydrogen content is set to the beginning-of-life value if the Cr has not yet been fully consumed. If the Cr has been fully consumed, the empirical function of burnup used for uncoated cladding is applied, but with the burnup replaced by an effective burnup equal to the actual burnup minus the burnup at which the Cr becomes fully consumed.

[5] with zirconium also diffusing into the intermetallic layer, resulting in an interdiffusion process (necessarily, to obtain the $ZrCr_2$ stoichiometry).

[6] the relevant accidents for fuel performance modelling, which generally have maximum cladding temperatures below ~ 1300 °C by design; eutectic formation and clad melting are important for beyond-design-basis (severe) accidents, but these are modelled using severe accident codes like MELCOR and MAAP, which simulate the overall degradation behaviour of the core.

coefficient of Cr in β-Zr, C_{init} is the initial Cr concentration in the base alloy, and $C_s = C_s(T)$ is the saturation concentration of Cr in β-Zr. The result is (Brachet, et al., 2019)[7]

$$C(x,t) = (C_s - C_{init})\left[1 - erf\left(\frac{x}{2\sqrt{Dt}}\right)\right] + C_{init} \quad (3)$$

where erf is the error function. The number of Cr atoms lost from the coating per unit length,

$$a_{lost} = 2\pi r_{int}\int_0^{\infty}(C(x,t) - C_{init})dx \quad (4)$$

where r_{int} is the coating-base alloy interface radius, which has the solution

$$a_{lost} = 4\pi r_{int}(C_s - C_{init})\sqrt{\frac{Dt}{\pi}} \quad (5)$$

Also,

$$C = \frac{w}{100}\frac{\rho_{base}}{52u} \quad (6)$$

where w is the Cr concentration as a percentage of the base alloy weight, ρ_{base} is the base alloy density, and u is the unified atomic mass unit, and, equating Cr atoms lost per unit length with the Cr atoms per unit length in the thickness of Cr, x_{lost}, that is lost,

$$2\pi r_{int}x_{lost}\frac{\rho_{Cr}}{52u} = a_{lost} \quad (7)$$

where ρ_{Cr} is the density of chromium in the coating.

Combining Equations (5), 6 and 7,

$$x_{lost} = \frac{2(w_s - w_{init})}{100}\frac{\rho_{base}}{\rho_{Cr}}\sqrt{\frac{Dt}{\pi}} \quad (8)$$

where $w_s = w_s(T)$ is the saturation weight percentage of Cr in β-Zr, and w_{init} is the initial weight percentage of Cr in the base alloy.

Unfortunately, Equations (3) to (8) do not apply to a multi-timestep scenario where temperatures vary from timestep to timestep. Thus, the approach above of evaluating Cr diffusion and thinning of the Cr coating cannot be employed in ENIGMA (or any other fuel performance code). Instead, a finite difference approximation to Equation (2) is solved on a substep-by-substep and axial-zone-by-axial-zone basis, with concentration, C, replaced by weight percentage, w; that is,

$$\frac{\partial w}{\partial t} = D\frac{\partial^2 w}{\partial x^2} \quad (9)$$

is solved.

For each axial zone in ENIGMA, the cladding base alloy thickness (which is treated as a plane wall) is discretised by N + 2 nodes, with node 0 at the clad bore, node N + 1 at the base alloy-coating interface, and N base alloy nodes inbetween. Given the strong increase in chromium weight percentage gradient as the interface is approached, the number of nodes for an accurate solution is minimised by a non-uniform node spacing whereby the separation, Δx_i, of node i at distance x_i from the clad bore and node i-1 at distance x_{i-1} from the clad bore is decreased according to a geometric sequence as i is increased; that is, $\Delta x_{i+1} = \alpha\,\Delta x_i$, where α (which must be less than unity) is the common ratio of the geometric sequence.

For each substep and axial zone, the end-of-substep Cr weight percentages at base alloy nodes 1 to N, w_1 to w_N, are computed as a function of the corresponding start-of-substep Cr weight percentages, $w_{1,p}$ to $w_{N,p}$, based on the current substep length, Δt, cladding metal-oxide interface temperature, T, saturation weight percentage of Cr in β-Zr, w_s, and Cr diffusion coefficient in β-Zr, D. The end-of-substep coating thickness loss due to Cr diffusion, x_{lost}, is then computed by numerical integration of the end-of-substep nodal Cr concentrations over the base alloy volume using the trapezoidal rule.

The start-of-substep Cr weight percentages are set to the as-manufactured Cr weight percentage in the base alloy, w_{BOL}, at beginning of life. w_{BOL} is in turn set to 0.1 for Zircaloy-2 and Zircaloy-4 (Allegheny Technologies Incorporated ATI, 2015), and to zero for ZIRLO®, Optimized ZIRLO™ and M5® (Halligan et al., 2015; Mardon et al., 2010).

w_{N+1} is set equal to w_s. w_s is in turn set by linear interpolation (with respect to temperature) of datapoints from the Zr-Cr phase diagram (Okamoto, 1993), with an empirical reduction of 0.5 based on experimental data for the saturation weight percentage in Zircaloy-4 (Brachet et al., 2019).

From the boundary condition that $\partial w/\partial x = 0$ at $x = 0$, w_0 is set equal to w_1.

D is calculated using a standard Arrhenius expression whereby

$$D = D_0 exp\left(-\frac{E}{kT}\right) \quad (10)$$

where $D_0 = 7.334\text{x}10^{-6}\ m^2s^{-1}$ is a multiplier, E is the activation energy for Cr diffusion, k is Boltzmann's constant, and $E/k = 20241$ K. The values of D_0 and E/k are fitted to data from experiments performed at Karlsruhe Institute of Technology (KIT) in Germany (Yang, et al., 2021), as described further below.

Calculations are only performed if (a) the start-of-substep coating thickness loss due to both oxidation and Cr diffusion is less than the as-manufactured coating thickness; and (b) the temperature, T, is greater than or equal to the β-Zr transition temperature. Otherwise, the end-of-substep Cr weight percentages in each node and coating thickness loss due to Cr diffusion are set to their start-of-substep values. For consistency with the Zr-Cr phase diagram data used, the β-Zr transition temperature is set to 831 °C.

Similarly, the calculation is repeated iteratively with a reduced substep length if the end-of-substep coating thickness loss due to both oxidation and Cr diffusion (with the former estimated by the start-of-substep value) is greater than the as-manufactured coating thickness. The substep length is first halved, and then subsequent guesses for substep length are obtained by bisection. The iteration is terminated when the end-of-substep coating thickness loss due to both oxidation and Cr diffusion is within 0.5 nm of the as-manufactured coating thickness.

The $\partial^2 w/\partial x^2$ term in Equation (9) is approximated by a central finite difference (Cheney & Kincaid, 1985), while the $\partial w/\partial t$ term in Equation (9) is approximated by a forward finite difference scheme.

The number of Cr atoms lost from the coating per unit length,

$$a_{lost} = 2\pi r_{int}\left(\sum_{i=1}^{N+1}\left[\frac{1}{2}(C_{i-1} + C_i)\Delta x_i\right] - C_{init}t_{base}\right) \quad (11)$$

Thus, from Equations (6) and (7),

$$x_{lost} = \frac{\rho_{base}}{100\rho_{Cr}}\left(\sum_{i=1}^{N+1}\left[\frac{1}{2}(w_{i-1} + w_i)\Delta x_i\right] - w_{init}t_{base}\right) \quad (12)$$

with ρ_{base} set using existing ENIGMA values for the different base alloys, and with ρ_{Cr} set to 7140 kg/m^3 (National Institutes of Health (2021b)).

As noted above, D_0 and E/k are fitted to data from experiments performed at KIT using data from (Yang, et al., 2021). These experiments involved isothermal annealing in an inert atmosphere (that is, with no oxidation) of specimens cut from Cr-coated Zircaloy-4 cladding tubes. Tests were performed at 1100, 1200 and 1300 °C for a number of different annealing times, and the post-test Cr and $ZrCr_2$ ("Cr-Zr interlayer") thicknesses were used to determine the proportion of the as-

[7] correcting a typographical error in the source reference.

manufactured Cr thickness that had been lost due to Cr diffusion into the base alloy ("dissolution"). The cladding tubes were coated with either a magnetron-sputtered (MS) chromium layer of 13 μm average thickness, or a cold-sprayed (CS) chromium layer of 32 μm average thickness.

The MS data were used to determine D_0 and E/k, and given the fluctuations in the CS data due to the irregularity of the coating thickness. Using Equation (8), the gradient of a linear regression fit of Cr thickness loss due to diffusion versus square root of annealing time at each temperature was multiplied by 100 $\rho_{Cr}\sqrt{\pi}$, divided by 2 (w_s-w_{init}) ρ_{base}, and then squared to give the diffusion coefficient, D, at that temperature (with ρ_{Cr}, w_s, w_{init} and ρ_{base} set as per the ENIGMA model). The results were 3.430, 5.545 and 22.892 $\mu m^2\ s^{-1}$ for temperatures of 1100, 1200 and 1300 °C. The ln D values were then plotted against inverse temperature, and a linear regression fit to the three datapoints gave an intercept of 15.808 $\mu m^2\ s^{-1}$ and a gradient of −20241 K. It follows that $D_0 = \exp(15.808) = 7.334x10^6\ \mu m^2\ s^{-1}$ and E/k = 20241 K.

The number of base alloy nodes, N, and the node separation common ratio, α, are inputs to the model for the coating thickness loss due to Cr diffusion. Optimised values to be used for the validation cases were determined by examining the effect of different values of N and α on the Cr thickness loss predictions from an ENIGMA simulation of the KIT test where an MS-coated specimen was annealed for 120 mins at 1200 °C (resulting in a measured loss of around half the coating thickness). Predictions converged towards a value of 7.11 μm (compare with the measured value of 6.2 μm) at large N and α values. Values of 20 and 0.95 were sufficient to give predictions equal to this asymptotic value to two significant figures.

2.3. Model for cladding creep

The model for creep of Cr-coated cladding was developed in two stages. Firstly, chromium creep data were reviewed and a thermal creep strain rate correlation for chromium was determined. This thermal creep strain rate correlation was then used in a new model for creep of a composite cladding where both the creep rates of the base alloy and chromium coating were combined to give a creep rate for the cladding as a whole.

Data relating to the high-temperature creep properties of pure chromium are scarce, due largely to the fact that it is typically used as an alloying element. The sources found relate to journal articles by Stephens and Klopp (1972), Kondo et al (1992, Kondo et al. (1993), and Allen (1966). All data are for tensile, uniaxial creep tests performed out of pile on unirradiated Cr wire or sheet samples. The Stephens and Klopp data were obtained for material with two different grain sizes – fine-grained material with an average grain diameter of 230 μm and coarse-grained material with an average grain diameter of 900 μm – in either a vacuum or an argon (inert) atmosphere at temperatures of 816 to 1316 °C and stresses of ~ 5 to 100 MPa. The Kondo data were obtained for material with a single grain size in either an air or argon atmosphere at temperatures of 900 to 1050 °C and stresses of ~15 to 70 MPa. The Allen data, which consist of a single measurement, were obtained for material with a single grain size in an argon atmosphere at a high temperature of 1550 °C and a low stress of 0.04 MPa. The Kondo data in air are affected by nitridation of the creep specimens, which has a significant impact on creep rate via solid solution strengthening. These data are therefore not considered further here, leaving only 1993 data at 1000 °C.

As per Ruano *et al* (Ruano et al. (1988), the chromium creep strain rate at low stress (LS) is assumed to be governed by a Harper-Dorn mechanism such that

$$\dot{\varepsilon}_{LS} = \frac{A_{LS} b D_L}{kT}\sigma, D_L = D_{0,L} exp\left(-\frac{Q_L}{RT}\right) \quad (13)$$

and the creep strain rate at high stress (HS) is assumed to be governed by a lattice and dislocation pipe diffusion driven power law creep mechanism such that

$$\dot{\varepsilon}_{HS} = \frac{A_{HS} D_{eff}}{b^2}\left(\frac{\sigma}{E}\right)^n, D_{eff} = D_{0,eff} exp\left(-\frac{Q_{eff}}{RT}\right) \quad (14)$$

where A_{LS}, A_{HS} and n are dimensionless constants, b is Burgers' vector, D_L is the lattice diffusivity, D_{eff} is the effective diffusivity for power law creep, σ is stress, E is Young's modulus, k is Boltzmann's constant, T is absolute temperature, $D_{0,L}$ and $D_{0,eff}$ are the lattice and effective diffusivity multipliers, Q_L and Q_{eff} are the lattice and effective diffusivity activation energies, and R is the molar gas constant.

The total creep strain rate,

$$\dot{\varepsilon} = \dot{\varepsilon}_{LS} + \dot{\varepsilon}_{HS} \quad (15)$$

Equations (13) to (15) are 'generic' equations which apply to 'consistent' stresses and strain rates, i.e. either a uniaxial stress and uniaxial strain rate, or a generalised stress and generalised strain rate.

The lack of a grain size dependence is consistent with the Stephens and Klopp data, where indistinguishable creep strain rates were obtained for the fine- and coarse-grained material at the same temperatures and stresses. However, it should be noted that this assumed grain size independence has not been validated with data for the low grain sizes representative of ATF material.

It is further assumed that (a) the lattice diffusivity and effective diffusivity are identical – that is, $D_{0,L} = D_{0,eff} = D_0$ and $Q_L = Q_{eff} = Q$; (b) the Burgers' vector is 0.25 nm (Ruano, Wadsworth, & Sherby, 1988); and (c) Young's modulus can be described by Wagih *et al*'s expression (Wagih, Spencer, Hales, & Shirvan, 2018),

$$E = C_0 - C_1 T - C_2 T^2 \quad (16)$$

where $C_0 = 2.6411x10^5$ MPa, $C_1 = 10$ MPa K^{-1} and $C_2 = 2.50x10^{-2}$ MPa K^{-2}, which is in turn a fit to data obtained by Armstrong and Brown in the temperature range of 25 to 1250 °C (Armstrong & Brown, 1964).

Q is set equal to the value of 73.2 kcal/mole (306.269 kJ/mole) determined by Stephens and Klopp. This is turn was based on chromium self-diffusion coefficient measurements made by Askill and Tomlin in 1964 (Askill & Tomlin, 1965). Fitting an equation of the form $D = D_0 \exp(-Q/RT)$ to these data (National Institute of Standards and Technology (2013)) with a Q value of 73.2 kcal/mole, a D_0 value of $1.55 \times 10^{-5}\ m^2\ s^{-1}$ was obtained.

Given the settings of b, E, Q and D_0 described above, the values of A_{LS}, A_{HS} and n were obtained by fitting Equation (15) to the combined (uniaxial) data for diffusivity-compensated creep strain rate (that is, creep strain rate divided by diffusivity) versus Young's-modulus-compensated stress (that is, stress divided by Young's modulus). The result, corresponding to A_{LS}, A_{HS} and n values of 8×10^{-10}, 2.5×10^{11} and 4.75, is illustrated in Fig. 2 (noting that 1823 K is the temperature to which the Allen datapoint corresponds). The A_{LS} value is based on the single low-stress datapoint of Allen, and the temperature dependence at low stresses has been assumed identical to that at high stresses due to lack of data. This means that the fitted creep model is subject to significant uncertainty at low stresses.

The fitted Equation (15) (with fitted constants A_{LS}, A_{HS} and n) is used 'as is' in ENIGMA for the creep of chromium with stresses and strain rates calculated consistently as generalised values.

The predicted creep rate versus stress behaviour of chromium at 1000 °C relative to that of Zircaloy-4 and M5® base alloys (as predicted by the Donaldson and Kaddour-Massih high-temperature creep correlations (Rossiter and Peakman, 2024)) is illustrated in Fig. 3 and Fig. 4 (for a biaxial stress state applied to cladding tubes of typical dimensions via internal pressurisation). The much higher creep strength of chromium than of the base alloys is evident (in particular for base alloy material in the mixed α + β or β phases, which will quickly form at this temperature), and is a necessary requirement to explain the observed reduction in creep strain of Cr-coated cladding subjected to a high-temperature transient.

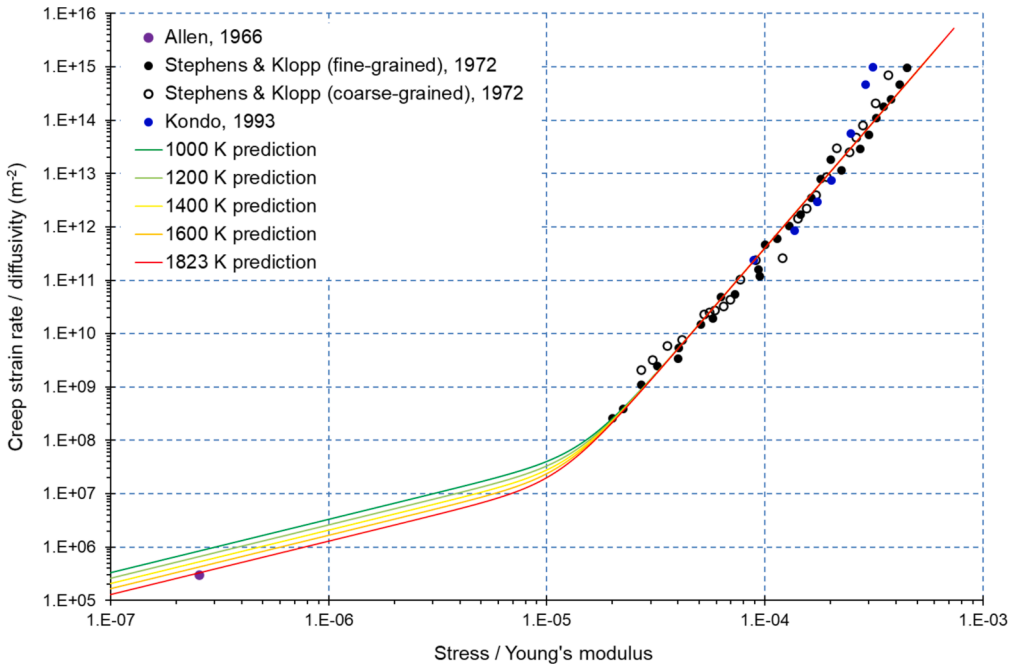

Fig. 2. Predictions and measurements of diffusivity-compensated creep strain rate versus Young's-modulus-compensated stress for chromium.

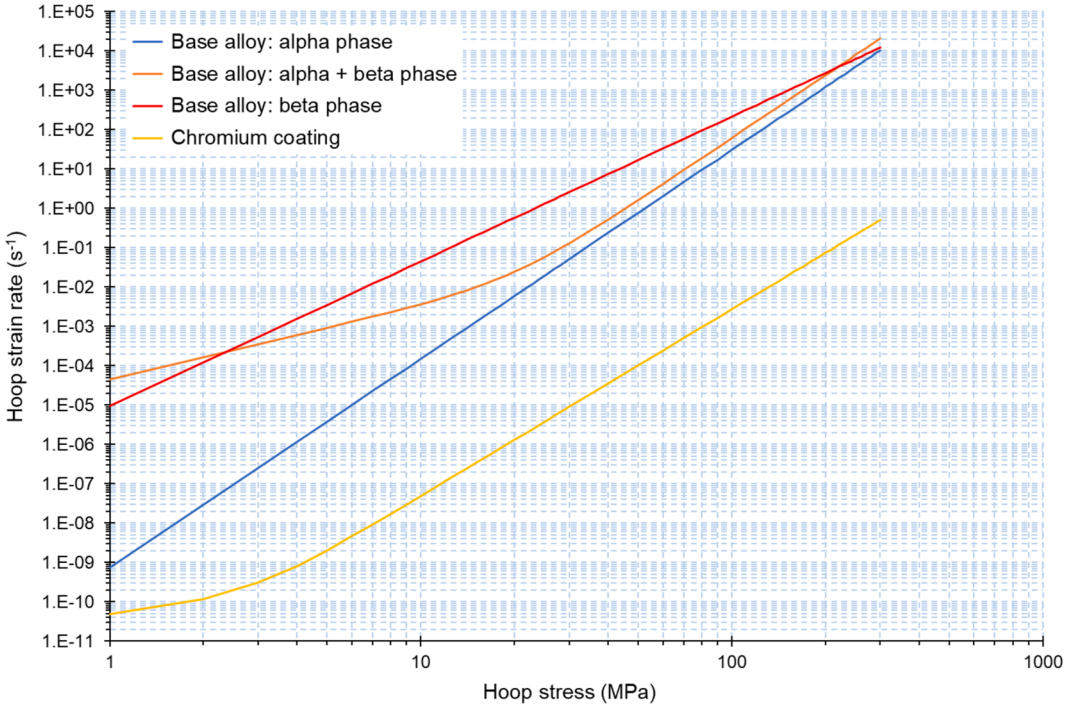

Fig. 3. Predictions of Cr and Zircaloy-4 creep rate versus stress behaviour at 1000 °C.

The new model for creep of a composite cladding sets creep strain rates as for the base alloy when the temperature is below the threshold for high-temperature creep (650 °C for M5® and 700 °C for all other base alloy types (Rossiter and Peakman, 2024)). This implicitly assumes that either (a) irradiation creep dominates in these conditions (as per normal operation with uncoated cladding) and irradiation creep strain rates for coated cladding are comparable to those for uncoated cladding (given the lack of data or an applicable correlation for irradiation creep of chromium, this is to some extent a necessary assumption); or (b) thermal creep dominates in these conditions (as per transients where high PCMI[8]-induced clad hoop stresses occur with uncoated cladding) but the overall cladding creep behaviour is similar for coated and uncoated cladding (again, given the lack of data or an applicable correlation for chromium creep at these low temperatures, this is to some extent a necessary assumption). In any case, this is consistent with the observation of reduced cladding creep for Cr-coated cladding being restricted to high-temperature conditions.

[8] pellet-cladding mechanical interaction

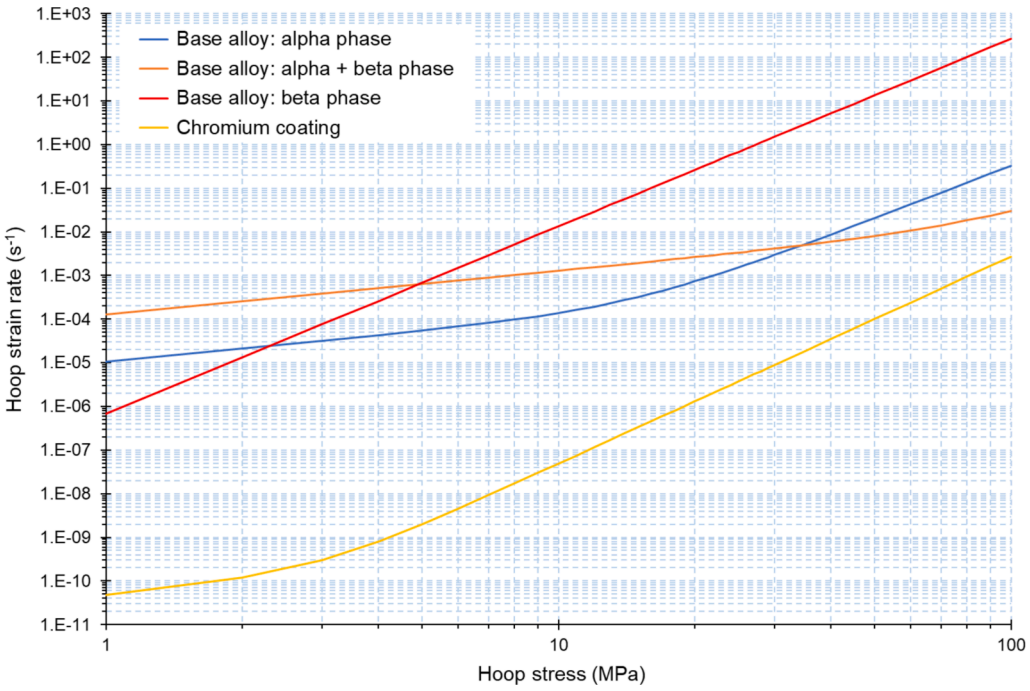

Fig. 4. Predictions of Cr and M5® creep rate versus stress behaviour at 1000 °C.

When the temperature is greater than or equal to the threshold for high-temperature creep, the coated cladding is assumed to behave as an integrated composite (that is, not as two distinct layers) whereby the generalised creep strain rate in a given timestep is equal in both base alloy and coating material. The generalised stresses in each material are then subject to the following relationship via the rule of mixtures (McLean, 1985):

$$\sigma = \sigma_c V_c + \sigma_b V_b \tag{17}$$

where σ is the generalised stress in the composite, which is equal to the applied generalised stress, σ_c is the generalised stress in the coating, V_c is the volume fraction of the coating, σ_b is the generalised stress in the base alloy, and $V_b = 1 - V_c$ is the volume fraction of the base alloy.

It follows that

$$\sigma_b = \frac{\sigma - \sigma_c V_c}{V_b} \tag{18}$$

and

$$\sigma_c = \frac{\sigma - \sigma_b V_b}{V_c} \tag{19}$$

The applied generalised stress is taken as an initial guess for both σ_c and σ_b and the coating and base alloy creep strain increments, $\Delta\varepsilon_c$ and $\Delta\varepsilon_b$, with these stresses are computed using the coating and base alloy creep strain rate correlations, with the coating correlation covering only thermal creep (irradiation creep of the coating is assumed to be negligible).

3. Validation

3.1. Validation cases

The validation of the chromium diffusion and coated cladding creep modelling is described below. Since the only usable data that are available for the oxidation of the chromium coating are the Framatome EATF data which are used to calibrate the oxidation model (see Section 2.1), there are (currently) no additional data available to independently validate the model. Thus, no validation of the coating oxidation model has been performed.

The chromium diffusion modelling was validated using data from experiments performed by the French Alternative Energies and Atomic Energy Commission (CEA) (Brachet et al., 2019; Brachet et al., 2020b). These experiments involved out-of-pile annealing of Cr-coated specimens in steam at a temperature of 1200 °C, and measurement of the resulting base alloy Cr weight percentage spatial distributions by EPMA. The specimens were unirradiated, and consisted of samples of coated Zircaloy-4 sheet (5–10 μm thick chromium coating deposited by PVD[9]) (Brachet, et al., 2019) and coated M5® cladding tube (12–15 μm thick chromium coating deposited by PVD) (Brachet et al., 2020a). Data are available for coated Zircaloy-4 specimens annealed for 10, 40, 160 and 280 s, and for a coated M5® specimen annealed for 1500 s.

A single ENIGMA run was performed to predict the base alloy chromium weight percentage distributions for the four coated Zircaloy-4 specimens. Since unfuelled sheet specimens cannot be simulated in ENIGMA, notional UO_2 fuel pellets were simulated together with coated Zircaloy-4 cladding of the same geometry as that in the KIT experiments used to develop the chromium diffusion modelling (see Section 2.2). This has no impact on the chromium diffusion calculations while allowing validation of the diffusion model as it is incorporated into ENIGMA, rather than on a stand-alone basis. Quasi-instantaneous heat-up to 1200 °C was modelled, followed by timesteps of 10, 30, 120 and 120 s to generate predictions at the experimental annealing times.

A second ENIGMA run was carried out to predict the base alloy chromium weight percentage distributions for the coated M5® specimen. Again, since unfuelled specimens cannot be simulated in ENIGMA, notional UO_2 fuel pellets were simulated. Quasi-instantaneous heat-up to 1200 °C was again modelled, followed by a timestep of 1500 s to generate predictions at the experimental annealing time.

Chromium diffusion only occurs – and is only modelled – at high temperatures relevant to accident conditions where β-Zr forms (as explained in Section 2.2). So there is no chromium diffusion during normal operation in LWRs, and no data or requirement to validate the chromium diffusion modelling in these conditions. Where chromium

[9] physical vapour deposition

diffusion does occur (high temperatures), no in-pile effects (over and above out-of-pile effects) are expected, but there are no validation data to prove or disprove this.

The coated cladding creep modelling was validated using data from an Electricité de France (EDF) semi-integral LOCA test of three Cr-coated Zircaloy-4 cladding tube specimens (Hazan, Gauthier, Pouillier, & Shirvan, 2021). The specimens had an inner diameter of 8.38 mm, an outer base alloy diameter of 9.5 mm, a chromium coating thickness of 25 μm (deposited via a cold spray technique), and a length of 300 mm. They were filled with alumina pellets, sealed with Zircaloy-4 end caps, and connected to a closed circuit which pressurised the specimens with argon at room temperature to a pressure of 50 bar. Testing was performed in EDF's semi-integral LOCA test facility, whereby each specimen is mounted vertically in an infra-red furnace within a sealed quartz test chamber through which steam is flowed. Quenching of the specimen is enabled by bottom-up filling of the test chamber with water. The experimental procedure consisted of heating in steam to 350 °C, holding at this temperature for a short time, applying a temperature ramp to 1200 °C at a rate of 10 °C s^{-1}, holding at 1200 °C for 176 s (specimen 1), 362 s (specimen 2) or 706 s (specimen 3), slow cooling (via turning off the furnace) to 700 °C, and rapid quenching (water fill rate of 25 mm s^{-1}) from 700 °C to ~200 °C. Rod internal pressure was measured online throughout the test. Clad ballooning and burst occurred in all cases during the temperature ramp, with clad oxidation occurring both during the ramp and the remaining test duration. Measured data relevant here include the rod internal pressures versus time (one specimen) and the post-test hoop strains (three specimens).

Since specimens and test conditions up until the end of the temperature ramp were identical, and burst occurred during the ramp in all cases, a single ENIGMA run was performed to predict the rod internal pressure, clad stress and clad strain versus time behaviour for the three coated specimens (with the maximum 706 s hold at 1200 °C applied, given the clad inner oxide thickness measurement was for the corresponding specimen). The alumina pellets were simulated as notional UO_2 fuel pellets, since the pellets have no effect on the cladding thermo-mechanical behaviour when there is no pellet heating, as in this case. For comparison purposes, and since measured post-test hoop strains are available (Hazan et al., 2021), a second ENIGMA run was carried out simulating the same tests but with an uncoated specimen that has the same geometry as the base alloy in the coated specimens.

Some additional specifics are important for the semi-integral LOCA test ENIGMA runs:

- The ENIGMA clad-stress-based failure model outlined in Ref. (Rossiter and Peakman, 2024) was employed. Given that initial scoping runs showed plastic instability was unrealistically limiting clad hoop strains at failure, the additional plastic instability strain rate failure criterion was set to an artificially high value of 100 s^{-1} to disable plastic instability failure (consistent with the approach taken in TRANSURANUS and BISON validation (Di Marcello et al., 2014; Pastore et al., 2021); a plastic instability failure criterion should in general only be applied for specific LOCA scenarios where the clad stresses are low (Di Marcello et al., 2014; Pastore et al., 2021)).
- As in previous LOCA modelling (Rossiter and Peakman, 2024), the Leistikow base alloy high-temperature oxidation model was used to align with the oxidation versus time and temperature assumption implicit in the clad-stress-based failure model.
- The pre-ballooning rod internal pressure increase observed during the testing was primarily driven by thermal expansion of argon in the closed circuit (Hazan et al., 2021), which is represented by an arbitrarily large plenum in the ENIGMA simulation. Thus, the (user-specified) plenum temperature was (a) increased to a value of 66.9 °C at a 350 °C specimen temperature that reproduced the measured pressure of 58 bar, and (b) further increased by 0.352 °C s^{-1} during the temperature ramp to reproduce the measured pressure increase rate prior to ballooning of ~0.006 bar per °C increase in specimen temperature.

3.2. Validation results

The measured and predicted end-of-test Cr weight percentage distributions for the CEA coated Zircaloy-4 sheet annealing experiments are shown in Fig. 5. Both measurements and predictions are provided for the four annealing times of 10, 40, 160 and 280 s. Similarly, the measured and predicted end-of-test Cr weight percentage distributions for the CEA coated M5® cladding tube annealing experiment (annealing time = 1500 s) are reproduced in Fig. 6. The agreement between measurements and predictions is in general good, albeit with a tendency for overprediction of Cr weight percentages, in particular at short annealing times. The predicted Cr diffusion coefficient at the temperature of 1200 °C relevant to these experiments is 7.91 $\mu m^2\ s^{-1}$. This compares with the value of 6.29 $\mu m^2\ s^{-1}$ used by CEA in generating their predictions (which agree almost perfectly with the measurements) for the coated Zircaloy-4 sheet annealing experiments (Brachet et al., 2019). This suggests that the tendency for overprediction is associated with an overprediction of Cr diffusion coefficient. However, diffusion coefficients are typically associated with relatively large uncertainties, and the diffusion coefficient formulation used in the ENIGMA model is derived from different experiments to those performed by CEA. Thus, the two values of diffusion coefficient are considered to be in good agreement, and the overpredictions of Cr weight percentages are well within the expected uncertainties.

The predicted behaviour of clad hoop stress versus time and clad plastic hoop strain versus time for the EDF semi-integral LOCA tests with coated cladding are shown in Fig. 7 and Fig. 8. Similarly, the predicted behaviour of clad hoop stress versus time and clad plastic hoop strain versus time for the EDF semi-integral LOCA tests with uncoated cladding are reproduced in Fig. 9 and Fig. 10. The clad hoop stress versus time figures also include plots of predicted clad failure (burst) stress versus time, and of the assumed clad temperature boundary condition versus time, while the clad plastic hoop strain versus time figures include only the latter.

The predicted behaviour is in all cases qualitatively in agreement with expectations. The clad plastic hoop strain increases more slowly with time for the coated cladding than for the uncoated cladding given the reduced creep rate. Thus, despite a slower reduction in failure stress with time due to the much reduced cladding oxidation, which increases the failure time and failure temperature, a significantly smaller clad strain is achieved for the coated cladding than for the uncoated cladding prior to cladding failure. Cladding failure temperature is somewhat overpredicted, at 904 °C for the coated cladding, and at 860 °C for the uncoated cladding, compared with average measured values of ~870 °C and 750 °C, respectively (Hazan et al., 2021). However, the cladding plastic hoop strain at failure is well predicted, at 14.9 % for the coated cladding and 30.7 % for the uncoated cladding, compared with average measured values of ~15 % and 35 %, respectively (Hazan et al., 2021).

The failure stress (Rossiter and Peakman, 2024) is calculated using the same model for both coated and uncoated cladding – that is, the failure stress model for uncoated cladding is assumed to also be applicable to coated cladding. The semi-integral LOCA test validation supports this approach, albeit only with one dataset.

Overall, the validation is successful, with the modelling approach for Cr-coated cladding broadly supported given the data currently available.

4. Future work

The work presented here has focused on the development of Cr-coated cladding models and their validation using two specific test cases: 1) out-of-pile annealing experiments conducted by CEA on Cr-coated Zircaloy-4 sheets and M5® cladding tubes, and 2) semi-integral

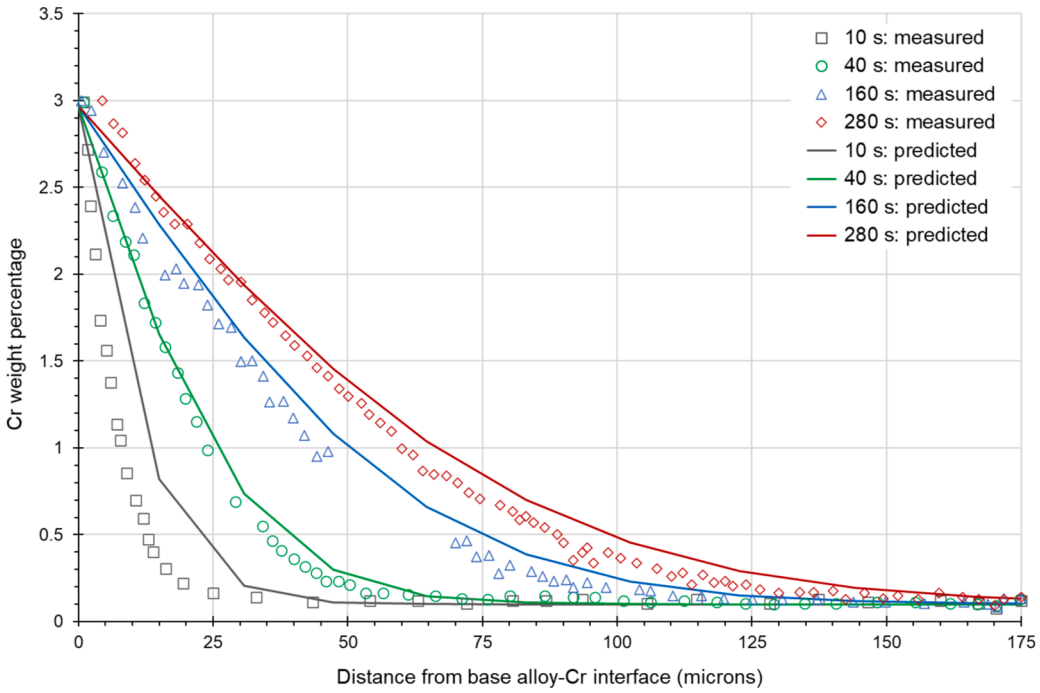

Fig. 5. Measurements and predictions of end-of-test chromium weight percentage distributions for CEA coated Zircaloy-4 sheet annealing experiments.

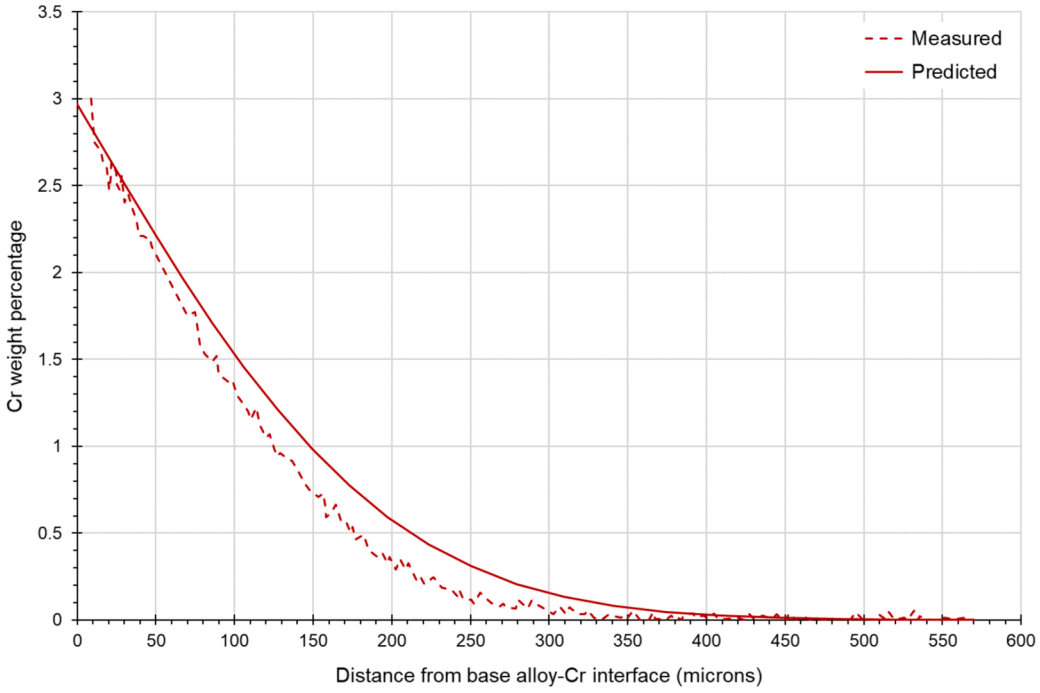

Fig. 6. Measurements and predictions of end-of-test chromium weight percentage distributions for CEA coated M5® cladding tube annealing experiment.

LOCA tests performed by EDF on Cr-coated Zircaloy-4. To date, there appears to be limited benchmarking of fuel performance codes using consistent validation cases for Cr-coated cladding. Notably, the two validation cases employed here are not widely used by other codes. Both TRANSURANUS and BISON have simulated the IFA 650.10 experiment as part of their model development, although it is important to highlight that the IFA 650.10 experiment was performed on uncoated cladding, and therefore the simulations using IFA 650.10 include an 'artificial' Cr coating layer not present in the original experiment (Aragon et al., 2025; Dunbar et al., 2024). Nevertheless, for benchmarking purposes, simulating the Cr-coated IFA 650.10 case is planned as part of a comparative study between ENIGMA and other widely used fuel performance codes. This will also provide an opportunity to incorporate uncertainties in input parameters and model parameters. Additionally, a sensitivity study on key model parameters would further enhance understanding of their impact on performance predictions.

It is recognised that for certain phenomena, additional validation would be very beneficial. In particular, the validation of creep behaviour for coated cladding remains limited and would benefit from further data being made available. Additional creep data for chromium and

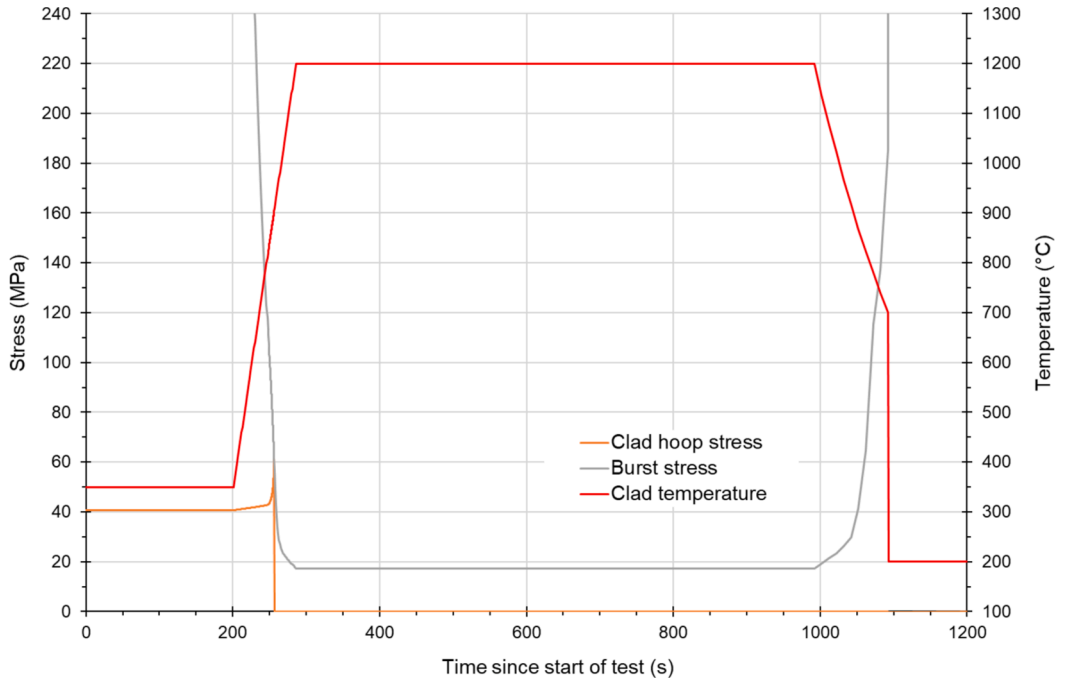

Fig. 7. Clad hoop stress versus time predictions for EDF semi-integral LOCA tests with Cr-coated Zircaloy-4 cladding tube specimens.

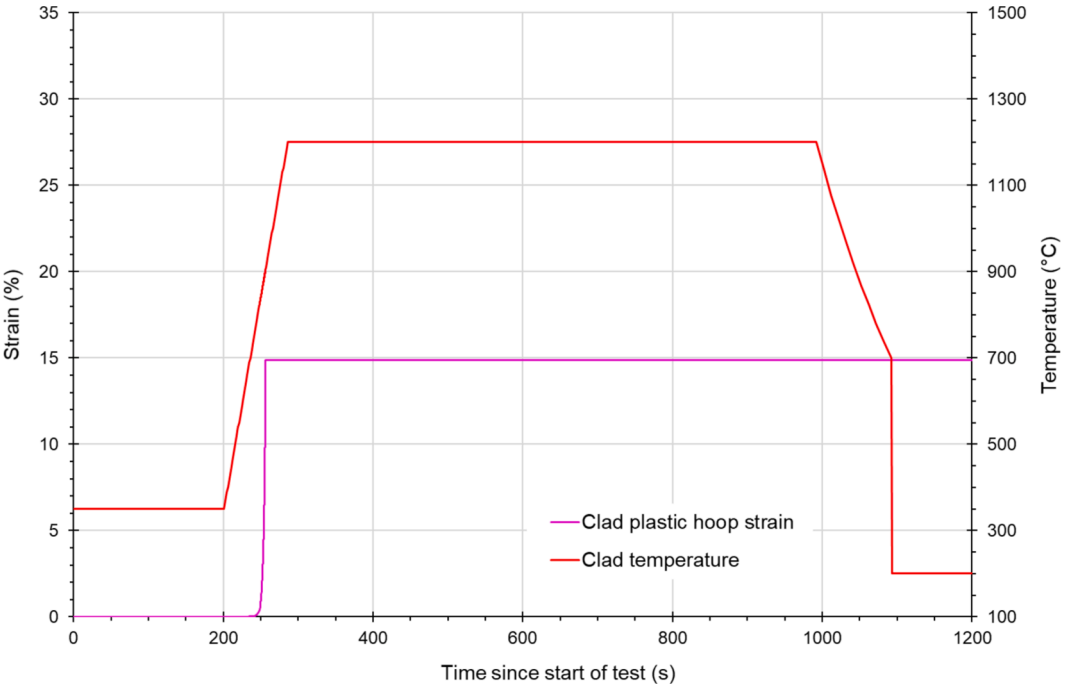

Fig. 8. Clad plastic hoop strain versus time predictions for EDF semi-integral LOCA tests with Cr-coated Zircaloy-4 cladding tube specimens.

chromium-coated zirconium alloys, particularly under low-stress conditions, are also necessary for model calibration. Moreover, further one-sided oxidation data on coated cladding tubes are required to improve validation of the coating oxidation model. These areas will be key priorities for future research to ensure comprehensive validation of the models.

5. Conclusions

As part of the continued development of the ENIGMA fuel performance code, significant enhancements have been implemented to enable modelling of chromium-coated zirconium-alloy cladding materials in LWRs. These enhancements were achieved by: 1) assessing the impact of the coating on cladding oxidation and hydriding using results from high-temperature oxidation tests on Framatome's Cr-coated M5® cladding, and using this assessment to develop modelling of cladding oxidation and hydriding at both low and high temperatures; 2) modelling the consumption of the coating layer due to Cr diffusion into the cladding base alloy's β-Zr phase at elevated temperatures, leveraging data from annealing experiments conducted by KIT in Germany; and 3)

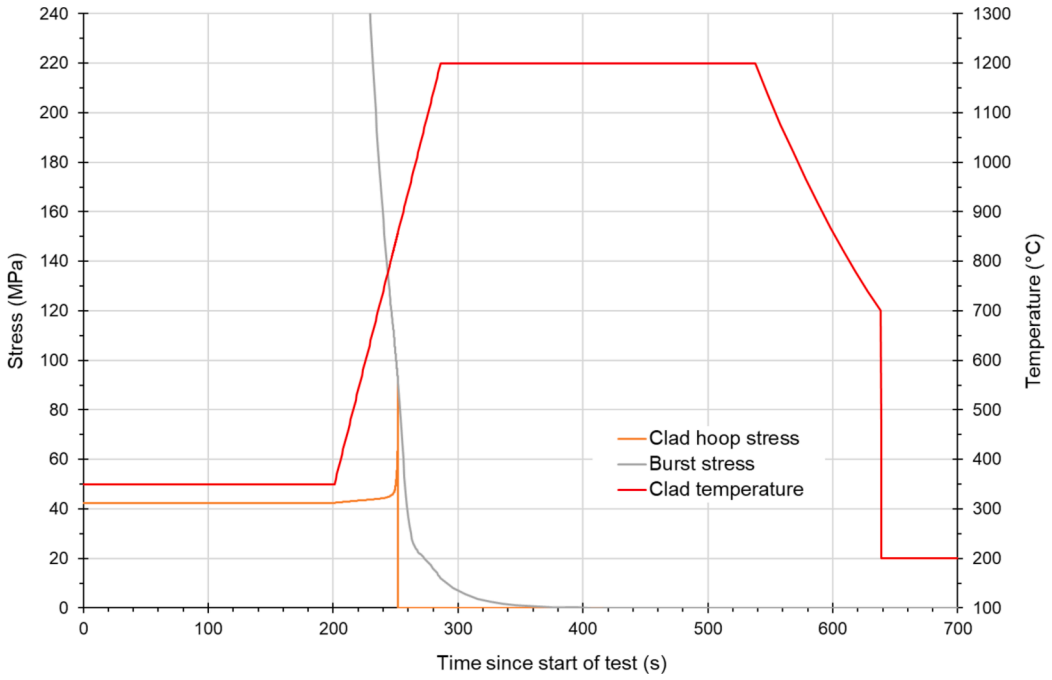

Fig. 9. Clad hoop stress versus time predictions for EDF semi-integral LOCA tests with uncoated Zircaloy-4 cladding tube specimens.

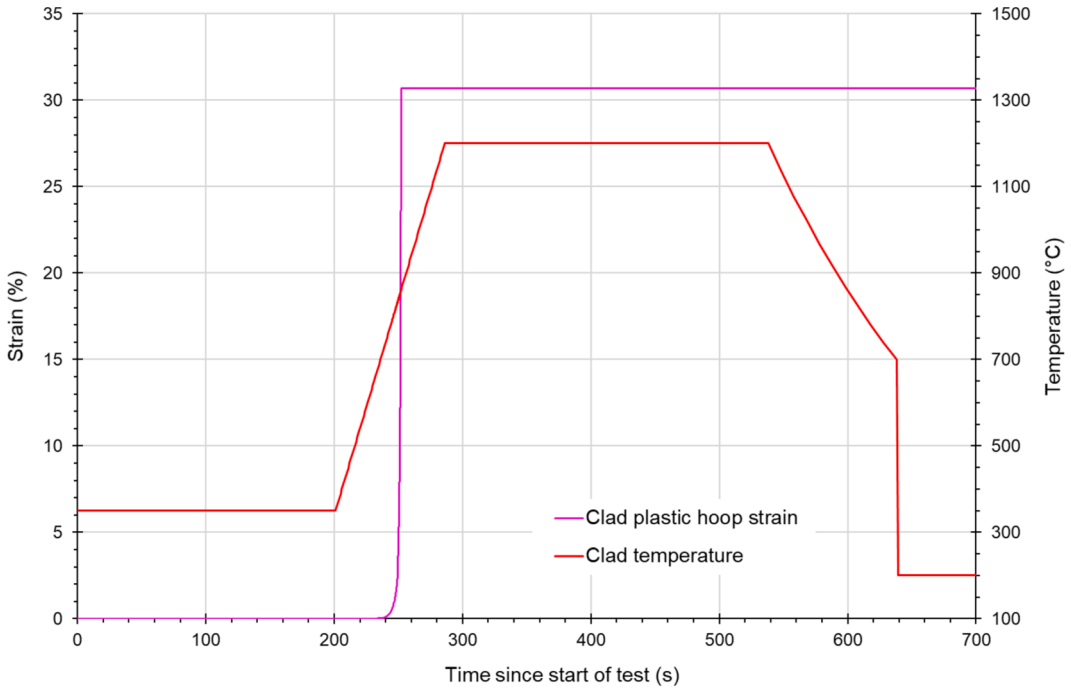

Fig. 10. Clad plastic hoop strain versus time predictions for EDF semi-integral LOCA tests with uncoated Zircaloy-4 cladding tube specimens.

incorporating low- and high-temperature cladding creep modelling based on chromium thermal creep data identified through a literature review.

The chromium diffusion modelling was validated using data from out-of-pile annealing experiments conducted by CEA on Cr-coated Zircaloy-4 sheets and M5® cladding tubes. The measured and predicted Cr concentration distributions after annealing at 1200 °C for various times (10, 40, 160, and 280 s for Zircaloy-4, and 1500 s for M5®) showed good overall agreement, despite a slight overprediction tendency at shorter annealing times. This discrepancy is attributed to differences in the chromium diffusion coefficients used in the ENIGMA model (as derived from KIT annealing experiments) and implied by the CEA measurements.

The coated cladding creep model was validated using data from semi-integral LOCA tests carried out by EDF on three Cr-coated Zircaloy-4 cladding tube specimens. The ENIGMA predictions for clad hoop stress and plastic hoop strain as a function of time were in qualitative agreement with the expected behaviour. The results indicated a slower increase in plastic hoop strain for coated cladding compared to uncoated cladding due to the reduced creep rate, resulting in smaller absolute clad strain prior to failure. Although there was some overprediction in cladding failure temperatures, the predicted plastic hoop strains at

failure closely matched the measured values, supporting the applicability of the new cladding creep model and the use of the existing failure stress model for uncoated cladding.

Overall, the enhancements to the ENIGMA code presented here are critical for accurately evaluating the extension of 'coping time' achievable with Cr-coated zirconium-alloy cladding during design-basis accidents. The validation showed good agreement between ENIGMA's predictions and the experimental data, thereby demonstrating the applicability of the new models for simulating the performance of LWR fuel rods with chromium-coated cladding in both normal operation and accident conditions.

CRediT authorship contribution statement

Glyn Rossiter: Writing – review & editing, Writing – original draft, Software, Investigation, Funding acquisition, Conceptualization. **Kerr Fitzgerald:** Writing – review & editing, Writing – original draft, Methodology. **Aiden Peakman:** Writing – review & editing, Writing – original draft, Investigation, Funding acquisition, Conceptualization.

Declaration of competing interest

The authors declare that they have no known competing financial interests or personal relationships that could have appeared to influence the work reported in this paper.

Acknowledgements

The work presented here was supported by the UK government's Department for Business, Energy and Industrial Strategy, as part of the Nuclear Innovation Programme (Advanced Fuels - 1404/12/2017). Aiden Peakman also received funding via the Royal Society Industry Fellowship (INF\R1\221061).

Data availability

Data will be made available on request.

References

Allen, B.C., 1966. Effect of rhenium on the interface energies of chromium, molybdenum, and tungsten. Trans. Metall. Soc. AIME 236, 903–915.
Aragon, P., Feria, F., Herranz, L., Schubert, A., Van Uffelen, P., 2025. Fuel performance modelling of Cr-coated Zircaloy cladding under DBA/LOCA conditions. Ann. Nucl. Energy, 110950.
Allegheny Technologies Incorporated (ATI). (2015). *Zirconium alloys technical data sheet.* Version 1, 2/3/2015.
Armstrong, P.E., Brown, H.L., 1964. Dynamic Young's modulus measurements above 1000°C on some pure polycrystalline metals and commercial graphites. Trans. Metall. Soc. AIME 230, 962–966.
Askill, J., Tomlin, D.H., 1965. Self-diffusion in chromium. Philos Magazine: J. Theoretical, Exp. Appl. Phys. 11, 467–474.
Bischoff, J., Vauglin, C., Delafoy, C., 2016. Development of Cr-coated zirconium alloy cladding for enhanced accident tolerance. *TopFuel 2016*. ANS, Boise.
Bischoff, J., Delafoy, C., Vauglin, C., 2018. AREVA NP's enhanced accident-tolerant fuel developments: Focus on Cr-coated M5 cladding. Nucl. Eng. Technol. 223–228.
Brachet, J.-C., Idarraga-Trujillo, I., Le Flem, M., Le Saux, M., Vandenberghe, V., Urvoy, S., Sanchette, F., 2019. Early studies on Cr-coated Zircaloy-4 as enhanced accident tolerant nuclear fuel claddings for light water reactors. J. Nucl. Mater. 517, 268–285.
Brachet, J.C., Le Saux, M., Bischoff, J., Palancher, H., Chosson, R., Pouillier, E., Bossis, P., 2020a. Evaluation of Equivalent Cladding Reacted parameters of Cr-coated claddings oxidized in steam at 1200 °C in relation with oxygen diffusion/partitioning and post-quench ductility. J. Nucl. Mater. 533, 152106.
Brachet, J.-C., Rouesne, E., Ribis, J., Guilbert, T., Urvoy, S., Nony, G., Pouillier, E., 2020b. High temperature steam oxidation of chromium-coated zirconium-based alloys: kinetics and process. Corros. Sci. 167, 108537.
Cheney, W., Kincaid, D., 1985. Numerical Mathematics and Computing, second ed. Brooks/Cole Publishing Company.
Cross, T., 2018. *Development of LWR fuels with enhanced accident tolerance: EATF Phase 2 final scientific technical report, October 2016 – September 2018.* Framatome report FS1-0041211.
Di Marcello, V., Schubert, A., van de Laar, J., Van Uffelen, P., 2014. The TRANSURANUS mechanical model for large strain analysis. Nucl. Eng. Des. 276, 19–29.
Dunbar, C., Jung, W., Armstrong, R., Sridharan, K., Corradini, M., Yeom, H., 2024. Fuel performance analysis of Cr-coated Zircaloy-4 cladding during a prototypical LOCA event using BISON. Ann. Nucl. Energy, 110411.
Hadri, M., Trovato, V., Bialecki, A., Merk, M., Peakman, A., 2021. Assessment of high-electrification UK scenarios with varying levels of nuclear power and associated post-fault behaviour. Energies 1780.
Halligan, J.R., Pan, G., Garde, A., Norrell, J., 2015. PWR Fuel Performance and Key Developments in Material and Mechanical Design. TopFuel, Zurich, Switzerland.
Hazan, J., Gauthier, A., Pouillier, E., Shirvan, K., 2021. Semi-integral LOCA test of cold-spray chromium coated zircaloy-4 accident tolerant fuel cladding. J. Nucl. Mater. 550, 152940.
Kondo, Y., Kawasue, K., Namekata, J., Sakaki, T., Honda, A., 1992. High temperature creep properties of high purity chromium. Tetsu to Hagane (J. Iron and Steel Institute of Japan) 78 (6), 947–954.
Kondo, Y., Kawasue, K., Namekata, J., Sakaki, T., 1993. High temperature creep resistance of high purity chromium in argon. Tetsu to Hagane (J. Iron and Steel Institute of Japan) 79 (11), 1299–1304.
Krejčí, J., Kabátová, J., František, M., 2020. Development and testing of multicomponent fuel cladding with enhanced accidental performance. Nucl. Eng. Technol. 597–609.
Mardon, J. P., Garner, G. L., & Hoffmann, P. B. (September 2010). M5® a breakthrough in Zr alloy. *LWR Fuel Performance/TopFuel/WRFPM.* Orlando, USA.
McLean, M., 1985. Creep deformation of metal-matrix composites. Compos. Sci. Technol. 23, 37–52.
National Institute of Standards and Technology (NIST). (2013, July 8th). *Cr self-diffusion Askill and Tomlin 1965*. Retrieved November 23rd, 2021, from https://materialsdata.nist.gov/handle/11115/135.
National Institutes of Health (NIH). (2021, July 17th). *PubChem compound summary: chromium*. Retrieved July 19th, 2021, from https://pubchem.ncbi.nlm.nih.gov/compound/chromium.
National Institutes of Health (NIH). (2021, July 24th). *PubChem compound summary: chromium (III) oxide*. Retrieved July 27th, 2021, from https://pubchem.ncbi.nlm.nih.gov/compound/517277.
Nea, 2021. Advanced Nuclear Reactor Systems and Future Energy Market Needs. OECD, Paris.
Okamoto, H., 1993. Cr-Zr (chromium-zirconium) phase diagram update. J. Phase Equilib. 14 (6), 768.
Pastore, G., Williamson, R.L., Gardner, R.J., Novascone, S.R., Tompkins, J.B., Gamble, K. A., Hales, J.D., 2021. Analysis of fuel rod behavior during loss-of-coolant accidents using the BISON code: cladding modeling developments and simulation of separate-effects experiments. J. Nucl. Mater. 543, 152537.
Peakman, A., Gregg, R., Bennett, T., Casamor, M., Martinez-Quiroga, V., Freixa, J., Pericas, R., Rossiter, G., 2022. Multi-phyiscs framework for whole-core analysis of transient fuel performance after load following ina pressurised water reactor. Annals of Nuclear Energy 173, 109086.
Peakman, A., Rossiter, G., 2024. UO2-Mo Composite Fuel Model Development and Simulation Using the ENIGMA Code. In: *International Conference on Physics of Reactors (PHYSOR 2024)*. ANS, San Francisco, pp. 1792–1800.
Rossiter, G., 2011. Development of the ENIGMA fuel performance code for whole core analysis and dry storage assessments. Nucl. Eng. Technol. 43 (6), 489–498.
Rossiter, G., Peakman, A., 2024. Development and validation of Loss of Coolant Accident (LOCA) simulation capability in the ENIGMA fuel performance code for zirconium-based cladding materials. Nucl. Eng. Des., 112767
Ruano, O.A., Wadsworth, J., Sherby, O.D., 1988. Harper-Dorn creep in pure metals. Acta Metall. 36 (4), 1117–1128.
Steinbrück, M., Vér, N., Große, M., 2011. Oxidation of advanced zirconium cladding alloys in steam at temperatures in the range of 600–1200 °C. Oxid. Met. 215–232.
Stephens, J.R., Klopp, W.D., 1972. High-temperature creep of polycrystalline chromium. J. Less-Common Met. 27, 87–94.
Sweet, R., Mouche, P., Bell, S., Kane, K., Capps, N., 2022. Chromium-coated cladding analysis under simulated LOCA burst conditions. Ann. Nucl. Energy, 109275.
Wagih, M., Spencer, B., Hales, J., Shirvan, K., 2018. Fuel performance of chromium-coated zirconium alloy and silicon carbide accident tolerant fuel claddings. Ann. Nucl. Energy 120, 304–318.
WNA. (2024a). *Are there different types of nuclear reactor?* Retrieved from World Nuclear Association: https://world-nuclear.org/nuclear-essentials/are-there-different-types-of-reactor.
WNA. (2024b). *Plans For New Reactors Worldwide* . Retrieved from World Nuclear Association: https://world-nuclear.org/information-library/current-and-future-generation/plans-for-new-reactors-worldwide.
Yang, J., Stegmaier, U., Tang, C., Steinbrück, M., Große, M., Wang, S., Seifert, H.J., 2021. High temperature Cr-Zr interaction of two types of Cr-coated Zr alloys in inert gas environment. J. Nucl. Mater. 547, 152806.
Yang, J., Steinbrück, M., Tang, C., Große, M., Liu, J., Zhang, J., Wang, S., 2022. Review on chromium coated zirconium alloy accident tolerant fuel cladding. J. Alloy. Compd. 895, 162450.
Yook, H., Shirvan, K., Phillips, B., Lee, Y., 2022. Post-LOCA ductility of Cr-coated cladding and its embrittlement limit. J. Nucl. Mater., 153354